Warming-induced Contraction of Tropical Convection Delays and Reduces Tropical Cyclone Formation

Gan Zhang

Department of Atmospheric Sciences

University of Illinois at Urbana-Champaign

1301 W. Green Street, Urbana, IL 61801

Corresponding Author

Gan Zhang (gzhang13@illinois.edu)

Abstract

The future risk of tropical cyclones (TCs) strongly depends on changes in TC frequency, but models have persistently produced contrasting projections. A satisfactory explanation of the projected changes also remains elusive. Here we analyze the TCs in large-ensemble climate simulations and show that a warming-induced contraction of tropical convection delays and reduces TC formation. This contraction manifest as stronger equatorial convection and weaker off-equatorial convection. It has been robustly projected by climate models, particularly in the northern hemisphere. This contraction shortens TC seasons by delaying the poleward migration of the intertropical convergence zone. At seasonal peaks of TC activity, the equatorial and off-equatorial components of convection contraction are associated with TC-hindering environmental changes. Finally, the convection contraction and associated warming patterns also explain the ensemble uncertainty in projecting future TC frequency. This convection contraction escaped the scrutiny of previous TC-climate studies, and recognizing its roles can motivate coordinated research and solidify confidence in projections of future TC risk.

As anthropogenic warming rises sea levels, increases extreme precipitation, and strengthens the most intense storms[1,2], the future global risk of tropical cyclones (TCs) strongly depends on the changes in TC frequency[3]. Despite extensive studies over the past two decades, the projected changes in global TC frequency remain uncertain[1–3]. While most global climate models project a decrease in global TC frequency, a statistical-dynamical downscaling model[4] that assumes unchanged statistics of convective disturbances suggests an increase in global TC frequency[1]. The direction of projected changes also depends on model parameters[5,6] and input variables[7]. For example, a set of high-resolution (25-km) climate simulations suggest that future TC frequency increases[5] as surface warming generates more seeding convective disturbances[6]. The diverging projections limit confidence in scientific understanding and complicate climate risk management.

The slow progress in reconciling the projection differences is increasingly attributed to the lack of a theoretical framework that fully explains the simulated changes and helps falsify alternative model assumptions[1,3]. Most theories recognize the essential role of atmospheric convection in TC development and are formulated around the variables related to convective processes. One line of thought is framed around the warming-induced changes of the vertical mass flux[8]. It suggests that TC genesis is hindered by a reduction of time-mean upward mass flux[9–11] and potentially by an increase of upward mass flux per TC[12]. Another line of research emphasizes the increasing saturation deficit of a warmer troposphere and suggests that the drying suppresses TC development by slowing the saturation of the convection environment[13,14] and facilitating the ventilation of TC convection[15,16]. Lastly, an emerging research line suggests that TC frequency may increase due to ocean warming, which promotes convective activity (including TC-seeding disturbances[6]) and expands the latitudinal range of the TC-permitting environment[17,18]. Though all developed around convection changes, these research lines rarely intersect with each other, and their connections with large-scale climate changes have not been well explored.

When explaining the climate impacts on TC activity, another line of active research builds on the concept of the Hadley circulation[19–22]. The Hadley circulation is a global-scale overturning circulation characterized by equatorial ascent and subtropical descent. A key feature of the Hadley circulation is its concentrated equatorial convection, or the intertropical convergence zone (ITCZ). The ITCZ is at the center of global energy transport and embodies rich interactions with other weather-climate processes[23]. They collectively modulate the large-scale environment and dynamical pathways of TC development. Under anthropogenic warming, climate models and theoretical arguments suggest the Hadley circulation will weaken and expand poleward. Although these circulation changes can be complicated by natural variability[24], the projections have been adopted to explain the observed and simulated changes in TC activity in qualitative and hypothetical ways[20,22].

Despite the intense interest in the Hadley circulation, past TC-climate studies paid limited attention to the seasonal migration and future changes of tropical convection. In the current climate regime, the location of tropical convection dictates the configuration of the Hadley circulation[25,26], with the equatorial convection disfavoring TC development and the off-equatorial convection favoring TC development[27]. While the annual means of TC activity and tropical convection do not share the same latitudes, their seasonal cycles suggest a close association (Figure 1a). The seasonal migration of tropical convection generally follows the insolation and the maximum of tropospheric moisture content (or moist static energy). During the equinoctial seasons, the convection concentrates near the equator and contributes to diverging upper-level outflows that descend in both hemispheres (Supplementary Figure 1a). The poleward flanks of the ITCZ are characterized by mid-tropospheric dryness related to descending motion and strong vertical wind shear related to subtropical westerlies. As the ITCZ migrates away from the equator during solstitial seasons, the convection in the summer hemisphere intensifies and drives an intense overturning cell with air ascending in the summer hemisphere and descending in the winter hemisphere (Supplementary Figure 1c). Although mid-tropospheric dryness and high wind shear dominate the winter hemisphere, wet and low-shear conditions prevail in the summer hemisphere and favor TC development. Consequently, the spatial-temporal distribution of tropical convection effectively regulates the TC frequency (Figure 1a). Beyond the seasonal forcing, this TC sensitivity to the convection location holds for a wide range of perturbations around the current climate[18,27,28].

Under anthropogenic warming, an analysis of recent climate simulations[29,30] and past studies[31–35] suggest that tropical convection will contract toward the equator. In a large ensemble of TC-permitting climate simulations (Method), this contraction manifests as the strengthening of equatorial convection at the cost of the off-equatorial convection on the poleward flanks of the ITCZ (Figure 1b). The contraction is evident through seasons and is the most robust around the transition from the boreal spring to boreal summer. In the early part of TC seasons, this contraction delays the poleward migration of the ITCZ and hinders the circulation shift towards the TC-favoring state. The contraction is also evident in the simulations of Coupled Model Intercomparison Project Phase 6 (CMIP6)[30] (Supplementary Figure 2). Despite some inconsistency in the southern hemisphere, the CMIP6 simulations concur with the large ensemble simulation and suggests the contraction of tropical convection is a robust response to anthropogenic warming.

In the previous CMIP simulations, similar signals of the convection contraction have been identified in the annual mean[31,32] and the seasonal cycle[33–35]. This warming-induced contraction likely arises from an enhanced equatorial warming[36] and cloud radiative feedback[32,37], which sharpen the meridional gradients in moist static energy and the convection activity[33,35,38]. When viewed as a delay and an equatorward displacement of the seasonal migration of tropical convection, this contraction can also be interpreted as a response to the warming-induced enhancement of cross-equator energy transport from the autumn hemisphere to the spring hemisphere[34,39]. The projected contraction depends on the equatorial warming[35], as well as model details of moist static energy and vertical velocity profiles[40].

The robustly projected contraction of tropical convection has so far escaped the scrutiny of many TC-climate studies. The existing studies mostly examine the ITCZ around the peak TC seasons and focus on the intensity and latitude of the precipitation maximum. Yet the contraction of tropical convection has no apparent impact on the latitude of precipitation maximum at the peak TC seasons (Figure 1b). Instead, the contraction displaces the global ITCZ the most in the early part of TC seasons. Meanwhile, the focus on the precipitation maximum makes it hard to detect subtle changes in the latitudinal distribution of tropical convection (e.g., equatorial convection increases). Lastly, the total precipitation increases poleward of the ITCZ due to the warming-related increase of atmosphere vapor content and deepening of the troposphere[41]. For many precipitation-based metrics, this widespread wetting likely blurs the signal of the convection contraction (Supplementary Figure 3).

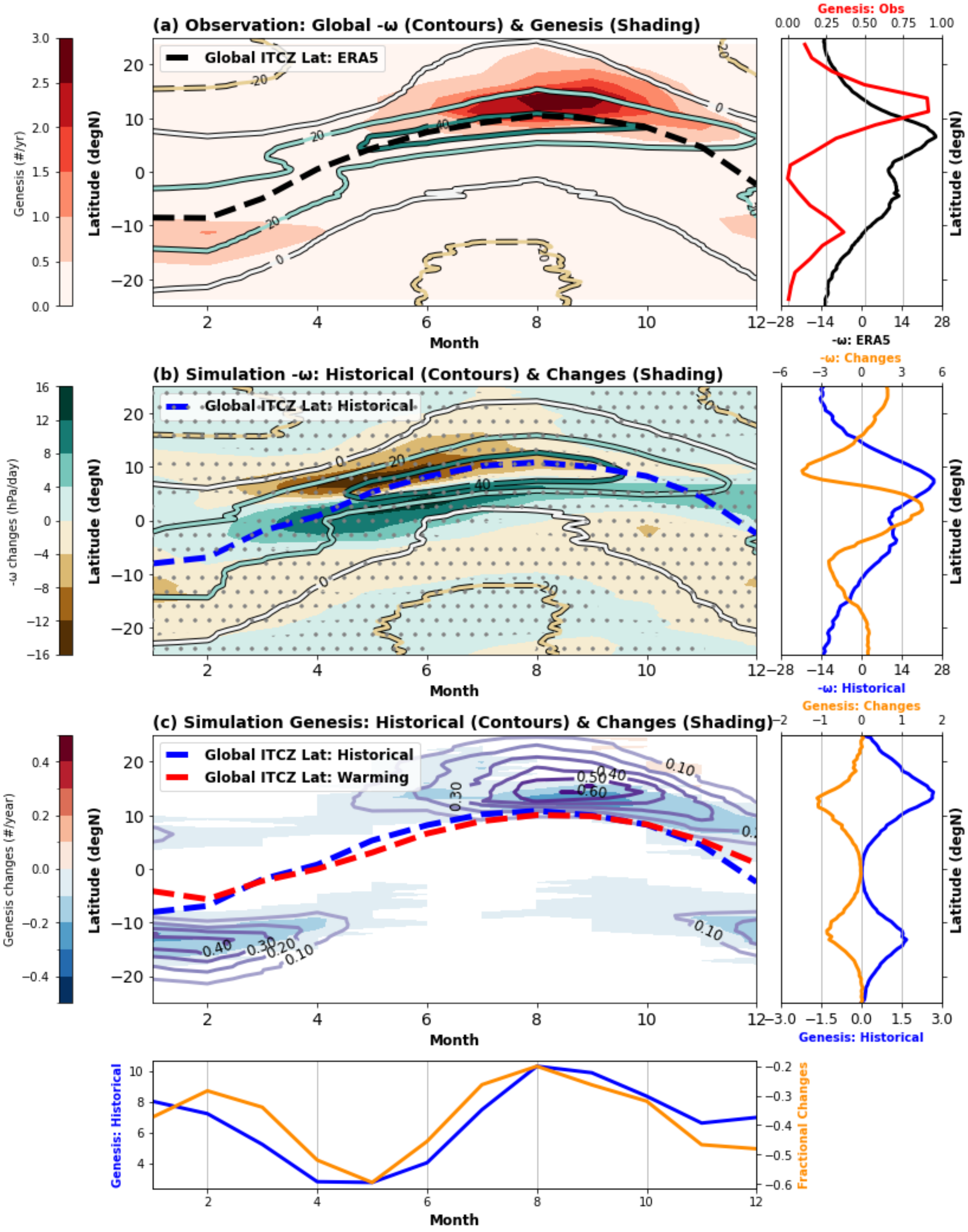

__Figure 1__ The observed and simulated monthly evolution of tropical convection and TC genesis frequency. (a) The 500-hPa vertical motion (-ω) (hPa day^{-1}; contours) from the ERA5 reanalysis and the TC genesis frequency (yr^{-1}; red shading) from the IBTrACS. The analysis uses -ω since negative ω values correspond to the upward motion. (b) The vertical motion in historical

simulation (contour) and its responses to the 4-K warming (warming - historical; shading) from the large ensemble simulations (Methods). The changes at the 99%-confidence level are marked with stippling. (c) The TC genesis frequency in historical simulation (contour) and its response to the 4-K anthropogenic warming (warming – historical; shading). The signals below the 99%-confidence are masked out. In (b-c), the mean latitudes of the weighted ITCZ (Method) of the reanalysis data (1981-2010), historical simulation (HPB), and warming simulation (4-K) are shown as black, blue, and red dashed lines, respectively. The vertical motion is zonal means, and the TC genesis is zonal sums. The annual means (right) and the meridional aggregations (bottom) of these quantities are displayed in auxiliary side panels. These quantities are denoted with colored axis labels.

The contraction of tropical convection is accompanied by a statistically significant decrease in the frequency of TC genesis (Figure 1c). This frequency decrease is qualitatively consistent with the impacts of stronger equatorial convection and weaker off-equatorial convection. Interestingly, the simulated TC decrease is season-dependent and mostly appears near the ITCZ. In the transition months of TC seasons (e.g., May-Jun in the northern hemisphere), the TC frequency decrease is relatively small in absolute values but represents a large fractional decrease. This feature suggests a possible shortening of the TC seasons associated with the delay of convection migration. Near the peak of TC seasons (e.g., Aug-Sep in the northern hemisphere), the TC frequency decrease is large in magnitude and preferentially occurs close to the ITCZ. This proximity suggests the TC frequency decrease is tied to the convection contraction, though the contributions of the equatorial and off-equatorial changes which will be discussed below. The ensuing discussion will examine the shortening of the TC seasons and the peak-season changes in detail.

Despite some biases in the simulated TC seasons (Supplementary Figure 4), the large ensemble simulation suggests that anthropogenic warming shortens and delays the TC seasons in individual basins (Figure 2). The probability distributions of TC genesis in the historical and warming simulations show differences with magnitudes up to ~0.15. Consistent with Figure 1c, individual basin often experiences a more pronounced suppression of TC activity in the transition seasons. If one defines the TC seasons with a 0.01-probability threshold of activity, the warming induced changes shorten the TC seasons by approximately 5-10%. Alternatively, the annual cycle can be divided into three-month periods consisting of a peak, a quiet, and two transitional seasons. Supplementary Figure 4 shows that the transition periods account for ~13% (North Atlantic) to ~200% (East Pacific) of the projected decreases in TC frequency, with the six-basin average being ~75%. This suggests the importance of transition periods despite some differences between basins.

Across the individual basins, one of the most consistent signals is the delay of the early part of TC seasons, which are around June for the northern-hemisphere basins and December for the southern-hemisphere basins. With the 4-K warming, the delay is fewer than 15 days in all the basins except for the East Pacific. Other less robust changes in the simulated seasonal cycle of TC activity include an enhanced concentration of TC genesis near the season peaks and a minor seasonal delay in the average time of TC genesis. For example, such seasonality changes are pronounced in the Northern Indian basin and alter the basin's bimodal distribution of TC geneses. The changes in this basin are consistent with Murakami et al[42] and the regional monsoon changes[43], though some quantitative aspects are likely model-dependent[44].

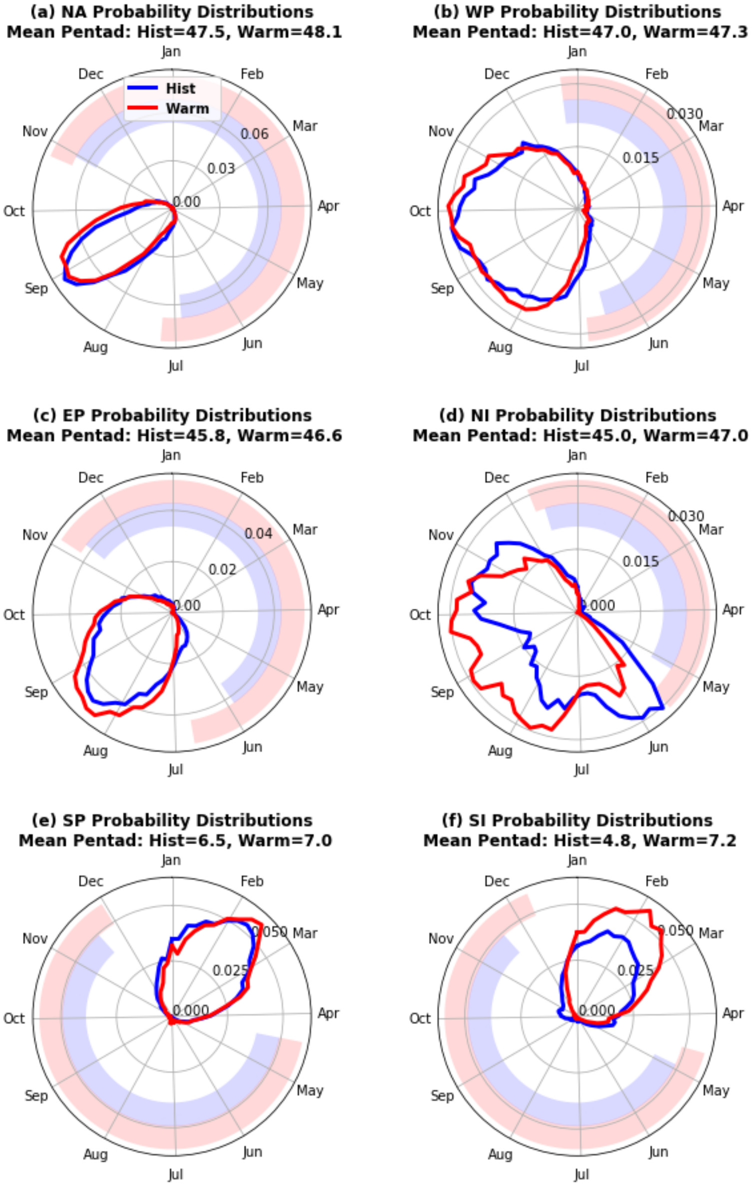

Figure 2 *The seasonal cycle of TC genesis in the historical and the warming simulations. The polar coordinates show the time of seasonal cycle and the annual probability distributions (unitless) in angular and radial axes, respectively. The probability distributions of TC genesis are shown as lines for the historical (blue) and warming (red) simulations. Six ocean basins are examined: (a) North Atlantic, (b) Northwestern Pacific, (c) Northeastern Pacific, (d) North Indian Ocean, € South Pacific, and (f) South Indian Ocean. The genesis time of individual TCs is grouped into 5-day bins (pentads) based on the corresponding day of the year (Method). The mean pentads*

in the historical and warming simulations are denoted at the top of subplots. The outer thickened arcs indicate the periods with suppressed TC activity defined with the 0.01-probability threshold (Method).

The simulated shortening and delay of the TC seasons are consistent with the responses to warming-induced convection contraction, but the observed and modeled changes in the TC season length can be complicated by other factors. For example, observational studies suggest the Atlantic TC season became longer[45] and started earlier[46] in recent decades, consistent with the concurrent increase in the number of Atlantic hurricanes and a large-scale environment more conducive for genesis[47]. It is possible that either natural variability[47] or anthropogenic forcings other than greenhouse gases (e.g., aerosols[48]) dominated the observed changes in an individual basin, especially as the current anthropogenic warming is substantially weaker than the 4-K warming. Another complication arises from a model that projects an increase in TC frequency[4]. When driven by the large-scale changes in the CMIP5 simulations, Emanuel's statistical-dynamic downscaling suggests the TC seasons become longer in most basins, in contrast to the results of climate models driven by the same CMIP5 changes . A recent examination of Emanuel's statistical-dynamical downscaling suggests that it tends to miss early- and late-season storms[50], implying some potential weakness representing the length of TC seasons. Meanwhile, the seasonal cycle in the large ensemble simulation is not perfect either (Supplementary Figure 4). A detailed assessment of the differences between our large-ensemble simulations and Emanuel's statistical-downscaling results is left for future research.

We next explore why TCs decrease near the ITCZ at the peak of TC seasons, as well as how it is related to the contraction of tropical convection. Recently, Hsieh et al[51,52] proposed that the variation in the TC frequency can be conceptually interpreted as a product of changes in the frequency of rotating convective disturbances (“seeds”) and the probability of disturbance-to-TC transitioning[51–53]. Hsieh et al[51,52] suggested that the former is correlated with the seed propensity index (SPI), and the latter inversely scales with the vertical wind shear and tropospheric dryness. We assume the SPI scales with the frequency of rotating convective disturbances[51,52,54] in the large ensemble simulation (Methods) and examine the latitudinal changes of the SPI, wind shear, and mid-tropospheric humidity (Method) at the peak of TC seasons. Given the active debate about the definition of TC “seeds”[51,54] and their role in the TC climatology[50], the upcoming discussion of the SPI serves as an example of linking existing hypotheses about future TC changes to the contraction of tropical convection.

Consistent with the peak-season decrease of TC frequency, the SPI decreases near the northern-hemisphere ITCZ (Figure 3a) and the poleward flank of the southern-hemisphere ITCZ (Figure 3c). The SPI changes arise primarily from the weakening of convection and the associated vorticity changes. More specifically, the weaker convection near 10°N and 15°S indicates less generation of low-level vorticity from the stretching of the atmosphere column. While the SPI’s vorticity term is also affected by the meridional gradient of vorticity, the local changes in vorticity generally prevail over the gradient changes induced by the contraction of tropical convection. The stronger equatorial convection and weaker off-equatorial convection are also accompanied by other environmental changes. For example, the contraction of tropical convection can dry the mid-troposphere[31] (Figure 3b) or enhance the vertical wind shear (Figure 3d) poleward of the ITCZ, which can suppress TC development via mechanisms independent of TC “seeds”.

The definition of the SPI and its intricate associations with other environmental factors warrant remarks. Specifically, the SPI is defined with a component of the vertical mass flux[51,52], which can be linked to convection changes, as well as surface fluxes and saturation deficit[50]. As suggested in the introduction paragraphs, those factors have been used to explain changes in future TC activity. One could argue that the projected changes in TC frequency may be attributed to the changes in vertical mass flux or moisture without invoking assumptions about the role of TC "seeds". While these physical hypotheses warrant future research, we speculate that the key environmental factor(s) will ultimately connect to changes in tropical convection, so our argument about the importance of the convection contraction will unlikely rest on the validity of a specific hypothesis.

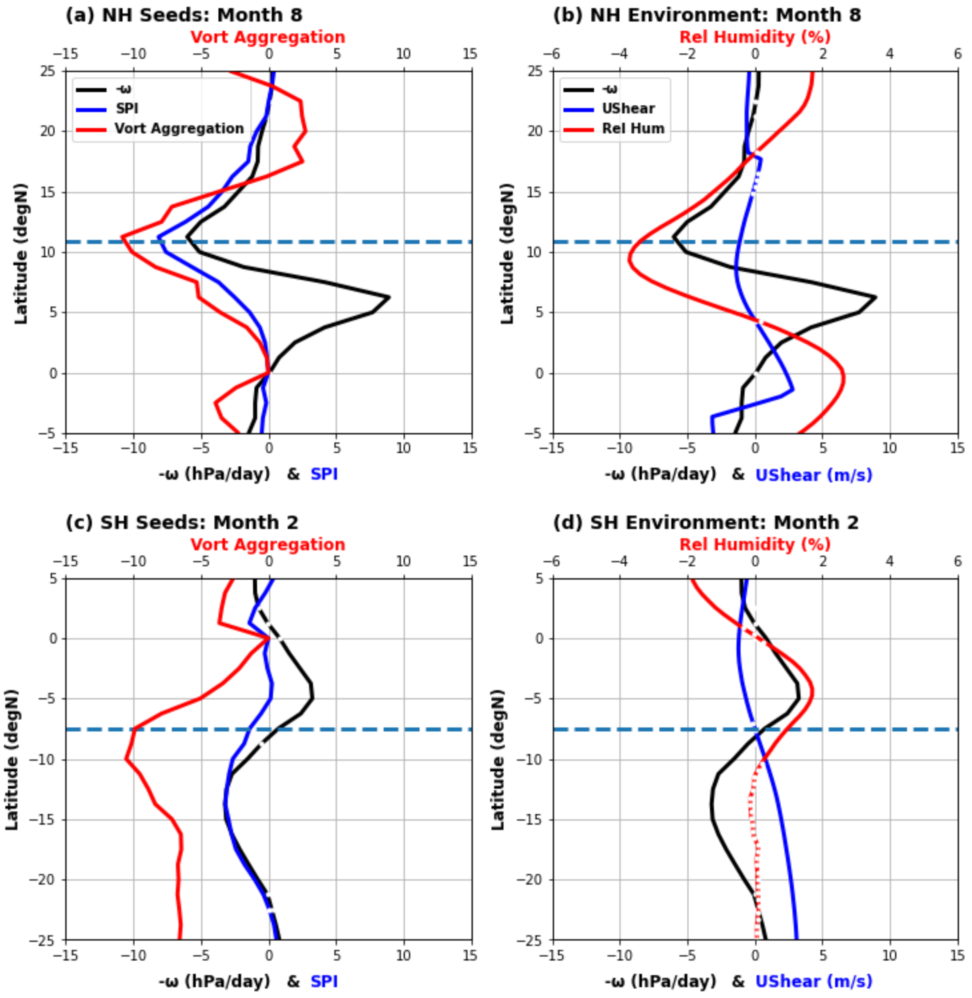

Figure 3 *Warming-induced changes in the latitudinal profiles of seed propensity index (SPI) and selected large-scale environmental variables. The results near the climatology peak of TC seasons*

in (a-b) the northern hemisphere and (c-d) the southern hemisphere are displayed separately. (a) August changes in the SPI and its two terms, namely the negative 500-hPa vertical motion and the 850-hPa vorticity aggregation. (b) August changes in the negative vertical motion (hPa day^{-1}*), mid-troposphere (600-hPa) relative humidity (%), and vertical shear of zonal wind (m s*$^{-1}$*). (c-d) are the same as (a-b), except for February changes. The horizontal dashed line indicates the latitudes of weighted ITCZ of the historical simulation (HPB) in the corresponding months. The changes below the 99% confidence level are marked with white breaks on the latitudinal profile lines.*

To further illustrate the importance of the convection contraction, we examine the relationship between the simulated changes (4K warming - historical) in the global TC frequency and tropical convection (Figure 4). This analysis leverages the large number of climate scenarios driven by natural and anthropogenic oceanic perturbations in the large ensemble simulation. Hence the analysis also offers an opportunity to examine the sensitivity of tropical convection and TC frequency to the patterns of surface warming.

Motivated by Figure 3, we partition the warming-induced contraction of tropical convection into equatorial and off-equatorial components. Overall, the equatorial convection strengthens while the off-equatorial convection weakens, suggesting the projected convection contraction is qualitatively robust. Nonetheless, details of the projected contraction are dependent on the warming patterns. For example, the convection changes in the southern hemisphere are relatively weak in simulations forced by two warming patterns (CC and GF; Methods). These simulations are likely responsible for the overall muted southern-hemisphere changes projected by the large-ensemble simulations (Figure 1b), which contrast with the projections by CMIP6 models

(Supplementary Figure 2). The inconsistency suggests larger uncertainty of our southern-hemisphere results. Compared to the other warming patterns (HA, MI, MP, and MR), the CC and GF warming patterns also show weaker El Niño-like warming in the tropical Pacific (Supplementary Figure 5), which likely affects regional TC activity together with changes in the South Pacific Convergence Zone[55]. Since the tropical Pacific warming profoundly affects the convection contraction[35] and may involve large model errors[56], it shall be a focus of future TC research.

Turning attention to TC frequency, the sign of peak-season changes is insensitive to the warming patterns, but the magnitude of these changes depends on these patterns and associated convection changes. In the northern hemisphere, the simulated changes in TC frequency are more closely correlated with the equatorial convection (0–7.5°N; r=0.35) than with the off-equatorial convection (8–20°N; r=0.30). The significant correlation between projected changes in the equatorial convection and TC frequency received limited attention from previous studies. The correlation with off-equatorial convection would strengthen if the simulations driven by the MI warming pattern are removed, though what makes the MI pattern distinct in driving TC changes is unclear. In the southern hemisphere, the correlation is weaker with the equatorial convection (0–7.5°S; r=-0.24) than with the off-equatorial convection (8–20°S, r=0.71). The strong correlation in the southern hemisphere (Figure 4d) may be surprising since a large area without TC activity (180°W-30°E) could render the changes in the global zonal means less relevant. The strong correlation with off-equatorial convection is contributed by the South Indian and the South Pacific basins. In particular, the South Pacific Convergence Zone shows a noteworthy equatorward displacement at the peak TC season (Supplementary Figure 6).

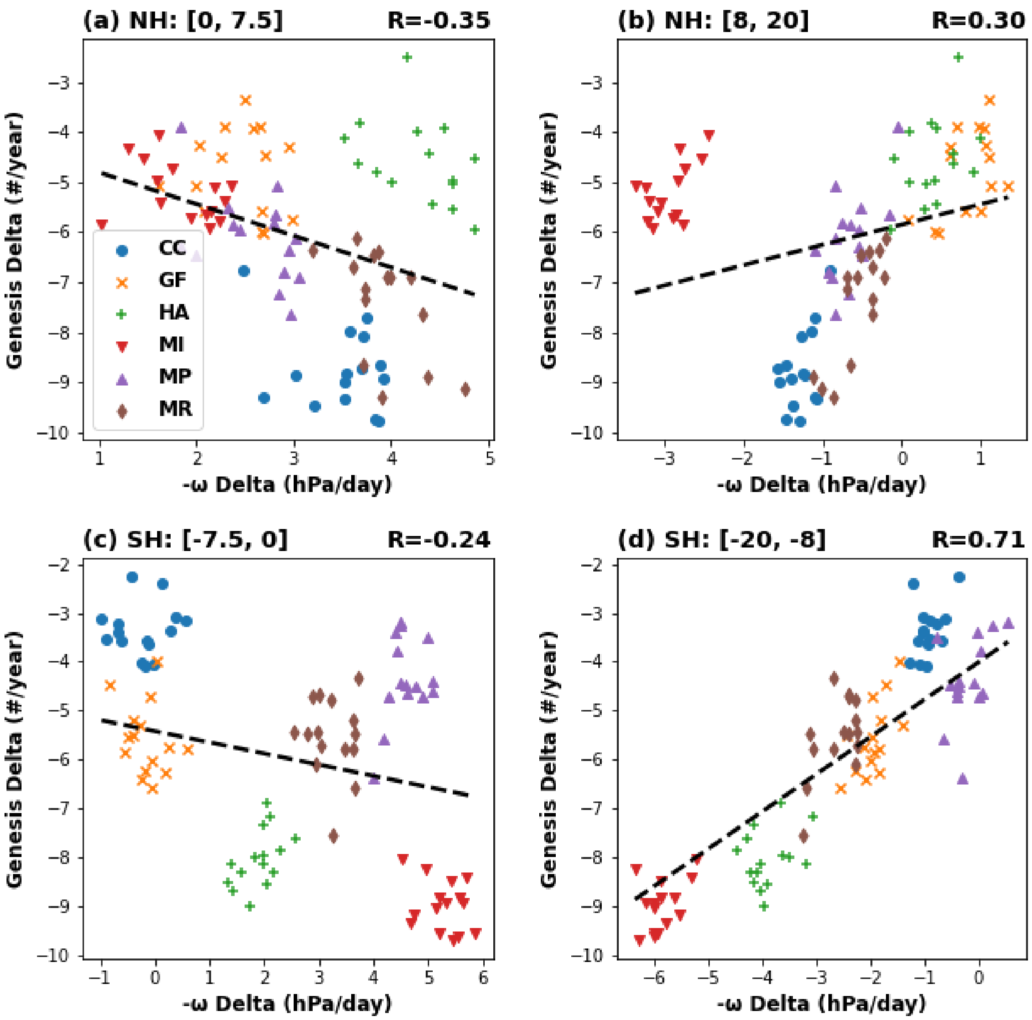

***Figure 4** Relationship between the warming-induced changes in the tropical convection (-ω at 500 hPa) and the global frequency of TC genesis. The evaluated months correspond to the peak TC seasons in (a-b) the northern hemisphere (August-October) and (c-d) the southern hemisphere (January-March). (a, c) Equatorial convection (0-7.5°) and (b, d) off-equatorial convection (8-20°) are evaluated for the hemisphere where the ITCZ and most TCs reside. The displayed changes are defined as the difference between the 4-K simulation and the ensemble mean of the historical simulations. Individual dots show ensemble members that are forced by six oceanic warming patterns (CC, GF, HA, MI, MP, and MR; see Method). The regression of ensemble members is*

shown with black dashed lines. The correlation coefficients (r) are shown in the upper right of corresponding subplots and are all above the 95% confidence level.

Recognizing the contraction of tropical convection and the inherent link between its off-equatorial and equatorial components helps identify new research topics. For weather-scale processes, the equatorial convection might suppress the nearby off-equatorial convection by stabilizing the troposphere and inducing downdrafts. Such a pattern of differential convective heating can either sustain a dynamically stable regime with aggregated convection and infrequent TC genesis[57] or result in dynamic instability that facilitates vortex roll-ups and periodic TC genesis[58,59]. Which scenario might prevail with anthropogenic warming warrants further investigation. From the climate perspective, the TC frequency decrease was often attributed to the weakening of tropical updraft, which has been considered as a circulation response needed to keep the global energy transport relatively stable when anthropogenic warming moistens the atmosphere[8]. Yet a contraction of tropical convection may also serve to satisfy the same energetic constraint[60]. When compensated by stronger equatorial convection, an additional reduction in the off-equatorial convection would be possible. To what extent this compensation occurs has apparent implications for the model-projected decrease in global TC frequency.

While some other factors in our discussion (e.g., weaker mass flux, mid-tropospheric drying, and fewer tropical disturbances) have been examined separately by previous studies, this study highlights that these factors can be consolidated into a conceptual framework centered on the tropical convection. Overall, the results of this study suggest that the contraction of tropical convection, which consists of stronger equatorial convection and weaker off-equatorial convection, is important for explaining the response of TC frequency to the anthropogenic warming simulated by climate models. The contraction delays the transition of atmospheric circulation to the TC-favoring state and potentially shortens TC seasons by 5-10% with 4-K warming. The changes in the transition season on average accounts for ~75% of the TC frequency decreased projected by the large ensemble simulation. During the core of TC seasons, the contraction suppresses the development of convective disturbances and makes the large-scale circulation deviate from the TC-favoring state. Although the convection contraction does not explicitly address the TCs at the tropical-extratropical interface, which poses an additional threat in a warmer climate[17,18], this contraction may exert an indirect influence via the upper-level outflow of the Hadley circulation and the subtropical westerlies[31].

Our attempt to analyze more high-resolution climate simulations[61,62] was hindered by data availability issues (e.g., missing variables). We thus acknowledge that our conclusions partly depend on the fidelity of the examined models in simulating the multi-scale physical processes and their changes due to the anthropogenic warming. At the same time, observational studies have found signals consistent with the simulated contraction, including a seasonal delay of tropical precipitation[63] and a contraction of the Pacific ITCZ[64]. Although this study does not seek to attribute the observed changes in global TC frequency, the observed contraction appears consistent with a declining trend in the number of TCs globally[22]. Finally, the convection contraction explains a substantial portion of the uncertainty in the projection of global TC frequency by the large-ensemble climate simulations (Figure 4). Further coordinated effort in theoretical development, climate modeling, and careful consideration of additional climate processes (e.g., the planetary waves and midlatitude circulations) will lead to increased confidence in projections of future TC risk.

Methods

Observational Data

The reference climate data in this study is the observation-constrained ERA5 reanalysis[65]. We use the monthly data on a 0.25-degree grid, which represent the tropical convection at a spatial resolution much higher than most earlier reanalysis datasets. The observational data of tropical cyclones (TCs) is the International Best Track Archive for Climate Stewardship (IBTrACS)[66]. For the sake of a relatively homogeneous definition of TC genesis across the global basins, we use the US-sourced subset of storm data in the IBTrACS. The historical analyses focus on the 30-year period of 1981-2010, which is covered by relatively reliable satellite observations and simulated by the most recent climate models.

Coupled Model Intercomparison Project (CMIP) Data

CMIP6 data are analyzed to illustrate the robustness of the convection traction. Our analysis uses a subset of models with high-resolution configurations (approximately 1-deg grid) available in the CMIP6[30] archive. The selected models include BCC-CSM2-MR, CMCC-CM2-SR5, CNRM-CM6-1-HR, CSIRO-ARCCSS-CM2, EC-Earth3, GFDL-CM4, HadGEM3-GC31-MM, MIROC6, MPI-ESM1-2-HR, MRI-ESM2-0, NCAR-CESM2, and TaiESM1. To facilitate comparison with the ERA5 reanalysis and the large-ensemble simulations, we use the Atmospheric Model Intercomparison Project (AMIP) simulations as the reference climate and the high-end Shared Socioeconomic Pathway (SSP5-85) simulations as the warming climate. Moreover, the strong forcing helps generate signals that are relatively easy to identify with single runs of climate models. This study also uses the CMIP5[67] data indirectly as their warming patterns serve as input for the large-ensemble simulations (see next section).

High-resolution Large Ensemble Simulation

The analyzed large-ensemble simulation is a subset of the Database for Policy Decision Making for Future Climate Change (d4PDF)[29]. The simulation is conducted using Meteorological Research Institute–Atmospheric General Circulation Model version 3.2 (MRI-AGCM3.2H)[68] on a grid with ~60-km grid spacing. The historical (1951–2010) simulation covers 1951-2010 and is driven by the observed forcings including the time-varying oceanic information. A 100-member ensemble simulation is generated by perturbing the initial conditions of the atmosphere and the sea surface temperature (SST). To account for observational uncertainties, the input SST forcing also includes random perturbations up to 30% of the observed interannual variability of the SST.

The future warming simulation uses the greenhouse gas forcing that corresponds to the 2090 values of the CMIP5's representative concentration pathway 8.5 scenario. Its input SST forcing is based on the detrended SST observations plus representative SST warming patterns from six CMIP5 models. The models include HadGEM2-AO, MPI-ESM-MR, MRI-CGCM3, NCAR-CCSM4, GFDL-CM3, and MIROC5 – and are denoted as HA, MP, MR, CC, GF, and MI in Figure 4. In these simulations, each warming pattern is scaled to be 4-K warmer relative to the preindustrial climate and then serves as input to generate a 15-member ensemble. The SST warming patterns vary seasonally, and Supplementary Figure 5 shows the annual means of these warming patterns. The model settings and the experiment design are described in detail by Mizuta et al.[29].

The large ensemble simulations produce a realistic historical climatology (including the large-scale environment and TC activity[69,70]) and a warming-induced reduction in the global TC frequency as most other climate models. This set of simulations consists of several unique advantages that are leveraged by this study. For example, the simulations contain exceptionally many ensemble members that are useful for accumulating TC samples, identifying warming-induced responses, and evaluating sensitivities across ensemble members. Besides helping simulate TCs, the high model resolution (for a climate model) is useful for the analysis of the convection changes near the narrow ITCZ. Finally, the model data, including TC information and key atmospheric variables, are meritoriously archived and publicly accessible.

Unless otherwise specified, all the key analyses in this study use the data of the large-ensemble simulation. The analyses focus on the 30-year climatology of the historical period (1981-2010) and 4-K warming scenario (2081-2110) to mitigate the burden of data management and avoid less reliable observational records. The warming-induced responses are defined as the 4-K warming (4-K) minus the historical (HPB) fields. The statistical significance of those responses is determined with the Student’s t-test using all the samples from the 100-member historical simulation and the 90-member warming simulation.

Definition of the ITCZ Latitude

This study determines the latitude of the ITCZ by calculating the centroid location of the tropical convection. For each month, an algorithm first identifies the grid points with top quartile convection within the latitude band of 25°S–25°N. Then the algorithm calculates the mean latitude of convection weighted by the convection intensity and the area of grid points. When the threshold excludes all grid points except for the maximum value, the search algorithm is equivalent to the commonly used metric of the ITCZ latitude, namely the latitude of tropical convection's maximum. In the transition seasons, the choice of using the top-quartile convection ensures a relatively robust definition of the ITCZ latitude when the convection maximum sticks with one hemisphere despite intense convection on the other hemisphere. The use of the top-quartile convection also excludes relatively weak convection outside the ITCZ (e.g., the subtropical precipitation). The output of this algorithm is robust against small changes in the percentile threshold.

TC Tracking and Genesis

Besides the IBTrACS observational data, the TC track data of the large-ensemble simulations[29] (doi:10.20783/DIAS.640) are also used.. The track data is archived by the Data Integration & Analysis System (DIAS) and provided by Yoshida et al[69]. The tracking algorithm, as described by Yoshida et al[69] and Murakami et al[71], is summarized as follows. The tracking algorithm considers multiple detection criteria about storm extremes and structure. It searches for candidate systems that meet certain thresholds for maximum relative vorticity and wind speed at the 850-hPa level. Additionally, the candidate systems are screened based on the presence of a warm core aloft and the vertical profile of wind speed. The screening in the Northern Indian Ocean also includes a specific check that differentiates TCs from monsoon depressions. When a candidate system meets all the criteria and lasts at least 36 hours, the algorithm classifies it as a TC. The detected TCs are then grouped based on genesis ocean basins. The threshold values used in the tracking process are identical to those of Murakami et al[71]. The values were chosen based on the model and ensures that the global number of detected TC geneses in the historical simulations and the observation are comparable.

We define the TC genesis as the first point of individual TC tracks. This definition circumvents the need of defining an intensity threshold of genesis or considering intensity biases of simulated TCs. However, an exact comparison between the observed and simulated TC geneses is hindered by differences between track methods. Since the observed TCs were mostly tracked by human forecasters and researchers, the tracking process changed over years and fundamentally differs from the automatic tracking applied to the large ensemble simulation. Such issues may moderately affect the analysis that involves the genesis location.

Analytics of the TC Seasonal Cycle

We analyze the TC seasonal cycle using the histograms of TC genesis time in individual basins. More specifically, we group all the simulated TCs in each TC basin for the historical and the warming experiments, respectively. In each basin, we convert the genesis time of individual TCs into the "day of year" and evaluate its histogram using 73 pentad (5-day) bins. Day 366 in the leap years of the 30-yr period is assigned to the first bin. To facilitate the comparison of the distribution shapes, we scale the histograms with the corresponding basin's total TC number in the historical or the warming experiments. Additionally, the periods of TC suppression (Figure 2) are defined as the pentad bins when <1% of a basin's TCs develop.

When paired with the large ensemble simulations, the analytical approach here has advantages in detecting shifts and yielding robust results. The use of pentad bins instead of monthly bins helps identify sub-monthly shifts in the TC seasons between the historical and the warming scenarios. This technique becomes feasible as the bundling of ensemble members ensures the large sample sizes of TCs. We have considered alternatives to define the TC seasons. For example, it is possible to define the TC season length using the difference between the genesis time of the first and the last TCs in the same season. But in the basins with low TC frequency, the stochastic noises and the warming-induced TC decrease can result in ill-defined TC seasons. For example, an extremely inactive season may generate zero or one TC, making the length of the TC season ambiguous.

Seed Propensity Index and the Large-scale Environment Analysis

Since the transfer and storage of the large-ensemble simulations make it computationally challenging to track rotating convective disturbances, we assume that their frequency scales with the Seed Propensity Index (SPI)[52]. The scaling relationship is valid with a few other high-resolution climate simulations when the SPI is defined as follows:

$$S = -\omega \frac{1}{1 + Z^{-1/\alpha}}$$

Where ω is the mean of isobaric vertical velocity at the 500-hPa level. The following term is referred to as the vorticity aggregation term in Figure 4 and scales with $Z^{1/\alpha}$ near the equator. Z is defined as:

$$Z = \frac{f + \zeta}{\sqrt{|\beta + \partial_y \zeta| U}}$$

Where f and β are the Coriolis parameter and its meridional gradients, and ζ represents the climatology relative vorticity at the 850-hPa level. The remaining parameters adopt the empirical fitting values $U = 20\ m\ s^{-1}$ and $\alpha = 0.69$ [52].

The original SPI definition uses zero values in regions with climatological subsidence (i.e., $\omega > 0$), but this could complicate the calculation and comparison of zonal means in different scenarios. For example, the regions with climatological convection can shift or change their size, making it difficult to directly compare the zonal means of SPI between different climate scenarios. To simplify the comparison, we calculated the zonal means without using zeros. This simplification mainly affects the subtropical regions with large zonal variations in the convection distribution. Near the equator, which is at the center of our discussion, the impact of this simplification is relatively small due to the widespread footprints of convection.

The analysis of the large-scale environment uses simple metrics, the vertical wind shear of zonal wind (200 hPa - 850 hPa) and the 600-hPa relative humidity, instead of the ventilation index as Hsieh et al. . This choice is a practical compromise related to the computational burden of calculating the ventilation index on a 60-km grid for nearly 6,000 simulation years. To conduct the calculation, the volume of input data will likely exceed 100 TB due to the involvement of vertical integrals and multiple physical variables. For our discussion of the global zonal means, we expect the results from the simple metrics to be qualitatively consistent with the results from the ventilation index.

Inclusion & Ethics

All the research data are publicly available, and the data sources have been acknowledged. All the individuals whose contributions do not meet the authorship criteria have been acknowledged.

Acknowledgment

The authors thank the science programs (SOUSEI, TOUGOU, SI-CAT, DIAS) of the Ministry of Education, Culture, Sports, Science and Technology (MEXT) of Japan for sharing the large ensemble simulation data and the tropical cyclone data (doi: 10.20783/DIAS.640). We also would like to acknowledge the data access and computing support provided by the NCAR CMIP Analysis Platform (doi:10.5065/D60R9MSP). Early discussions with Isaac Held and Adam Sobel helped motivate this study. GZ thanks Suzana Camargo, Tsung-Lin Hsieh, Thomas Knutson, Hiroyuki Murakami, and Yi Zhang for stimulating discussions that helped improve the study and its presentation. GZ also appreciates the support by the faculty start-up funds provided by the University of Illinois at Urbana-Champaign.

Data and Code Availability

The large ensemble climate dataset, including tropical cyclone tracks, is available via DIAS (https://diasjp.net/en/). The IBTrACS dataset is available via the National Centers for Environmental Information (https://www.ncei.noaa.gov/). The ERA5 reanalysis and CMIP data are accessible via the NCAR Research Data Archive (https://rda.ucar.edu/). The analysis code is available from G.Z. upon request.

Contributions

This study was conceived by G.Z. G.Z. acquired the data and performed the data analysis. G.Z. interpreted the results and wrote the manuscript.

Competing Interests

The authors declare no competing financial interests.

Corresponding author

Correspondence to Gan Zhang.

References

1. Knutson, T. *et al.* Tropical Cyclones and Climate Change Assessment: Part II: Projected Response to Anthropogenic Warming. *Bull. Am. Meteorol. Soc.* **101**, E303–E322 (2020).
2. Seneviratne, S. I. *et al.* Weather and Climate Extreme Events in a Changing Climate. in *Climate Change 2021: The Physical Science Basis. Contribution of Working Group I to the Sixth Assessment Report of the Intergovernmental Panel on Climate Change* 1513–1766 (Cambridge University Presss, Cambridge, United Kingdom and New York, NY, USA, 2021).
3. Sobel, A. H. *et al.* Tropical Cyclone Frequency. *Earths Future* **9**, (2021).
4. Emanuel, K. A. Downscaling CMIP5 climate models shows increased tropical cyclone activity over the 21st century. *Proc. Natl. Acad. Sci.* **110**, 12219–12224 (2013).
5. Bhatia, K., Vecchi, G., Murakami, H., Underwood, S. & Kossin, J. Projected Response of Tropical Cyclone Intensity and Intensification in a Global Climate Model. *J. Clim.* **31**, 8281–8303 (2018).
6. Vecchi, G. A. *et al.* Tropical cyclone sensitivities to CO2 doubling: roles of atmospheric resolution, synoptic variability and background climate changes. *Clim. Dyn.* **53**, 5999–6033 (2019).
7. Lee, C.-Y., Camargo, S. J., Sobel, A. H. & Tippett, M. K. Statistical–Dynamical Downscaling Projections of Tropical Cyclone Activity in a Warming Climate: Two Diverging Genesis Scenarios. *J. Clim.* **33**, 4815–4834 (2020).
8. Held, I. M. & Soden, B. J. Robust Responses of the Hydrological Cycle to Global Warming. *J. Clim.* **19**, 5686–5699 (2006).

9. Held, I. M. & Zhao, M. The Response of Tropical Cyclone Statistics to an Increase in CO2 with Fixed Sea Surface Temperatures. *J. Clim.* **24**, 5353–5364 (2011).
10. Sugi, M., Murakami, H. & Yoshimura, J. On the Mechanism of Tropical Cyclone Frequency Changes Due to Global Warming. *J. Meteorol. Soc. Jpn. Ser II* **90A**, 397–408 (2012).
11. Walsh, K. J. E. *et al.* Hurricanes and Climate: The U.S. CLIVAR Working Group on Hurricanes. *Bull. Am. Meteorol. Soc.* **96**, 997–1017 (2015).
12. Satoh, M., Yamada, Y., Sugi, M., Kodama, C. & Noda, A. T. Constraint on Future Change in Global Frequency of Tropical Cyclones due to Global Warming. *J. Meteorol. Soc. Jpn. Ser II* **93**, 489–500 (2015).
13. Emanuel, K., Sundararajan, R. & Williams, J. Hurricanes and Global Warming: Results from Downscaling IPCC AR4 Simulations. *Bull. Am. Meteorol. Soc.* **89**, 347–368 (2008).
14. Emanuel, K. Tropical cyclone activity downscaled from NOAA-CIRES Reanalysis, 1908–1958. *J. Adv. Model. Earth Syst.* **2**, 1 (2010).
15. Tang, B. & Emanuel, K. A Ventilation Index for Tropical Cyclones. *Bull. Am. Meteorol. Soc.* **93**, 1901–1912 (2012).
16. Tang, B. & Camargo, S. J. Environmental control of tropical cyclones in CMIP5: A ventilation perspective: VENTILATION OF CMIP5 TROPICAL CYCLONES. *J. Adv. Model. Earth Syst.* **6**, 115–128 (2014).
17. Studholme, J., Fedorov, A. V., Gulev, S. K., Emanuel, K. & Hodges, K. Poleward expansion of tropical cyclone latitudes in warming climates. *Nat. Geosci.* **15**, 14–28 (2022).
18. Zhang, G., Silvers, L. G., Zhao, M. & Knutson, T. R. Idealized Aquaplanet Simulations of Tropical Cyclone Activity: Significance of Temperature Gradients, Hadley Circulation, and Zonal Asymmetry. *J. Atmospheric Sci.* **78**, 877–902 (2021).

19. Zhang, G. & Wang, Z. Interannual Variability of the Atlantic Hadley Circulation in Boreal Summer and Its Impacts on Tropical Cyclone Activity. *J. Clim.* **26**, 8529–8544 (2013).

20. Kossin, J. P., Emanuel, K. A. & Vecchi, G. A. The poleward migration of the location of tropical cyclone maximum intensity. *Nature* **509**, 349–352 (2014).

21. Sharmila, S. & Walsh, K. J. E. Recent poleward shift of tropical cyclone formation linked to Hadley cell expansion. *Nat. Clim. Change* **8**, 730–736 (2018).

22. Chand, S. S. *et al.* Declining tropical cyclone frequency under global warming. *Nat. Clim. Change* **12**, 655–661 (2022).

23. Schneider, T., Bischoff, T. & Haug, G. H. Migrations and dynamics of the intertropical convergence zone. *Nature* **513**, 45–53 (2014).

24. Grise, K. M. *et al.* Recent Tropical Expansion: Natural Variability or Forced Response? *J. Clim.* **32**, 1551–1571 (2019).

25. Lindzen, R. S. & Hou, A. V. Hadley Circulations for Zonally Averaged Heating Centered off the Equator. *J. Atmospheric Sci.* **45**, 2416–2427 (1988).

26. Hack, J. J., Schubert, W. H., Stevens, D. E. & Kuo, H.-C. Response of the Hadley Circulation to Convective Forcing in the ITCZ. *J. Atmospheric Sci.* **46**, 2957–2973 (1989).

27. Merlis, T. M., Zhao, M. & Held, I. M. The sensitivity of hurricane frequency to ITCZ changes and radiatively forced warming in aquaplanet simulations. *Geophys. Res. Lett.* **40**, 4109–4114 (2013).

28. Ballinger, A. P., Merlis, T. M., Held, I. M. & Zhao, M. The Sensitivity of Tropical Cyclone Activity to Off-Equatorial Thermal Forcing in Aquaplanet Simulations. *J. Atmospheric Sci.* **72**, 2286–2302 (2015).

29. Mizuta, R. *et al.* Over 5,000 Years of Ensemble Future Climate Simulations by 60-km Global and 20-km Regional Atmospheric Models. *Bull. Am. Meteorol. Soc.* **98**, 1383–1398 (2017).

30. Eyring, V. *et al.* Overview of the Coupled Model Intercomparison Project Phase 6 (CMIP6) experimental design and organization. *Geosci. Model Dev.* **9**, 1937–1958 (2016).

31. Lau, W. K. M. & Kim, K.-M. Robust Hadley Circulation changes and increasing global dryness due to CO2 warming from CMIP5 model projections. *Proc. Natl. Acad. Sci.* **112**, 3630–3635 (2015).

32. Su, H. *et al.* Tightening of tropical ascent and high clouds key to precipitation change in a warmer climate. *Nat. Commun.* **8**, 15771 (2017).

33. Huang, P., Xie, S.-P., Hu, K., Huang, G. & Huang, R. Patterns of the seasonal response of tropical rainfall to global warming. *Nat. Geosci.* **6**, 357–361 (2013).

34. Song, F., Leung, L. R., Lu, J. & Dong, L. Seasonally dependent responses of subtropical highs and tropical rainfall to anthropogenic warming. *Nat. Clim. Change* **8**, 787–792 (2018).

35. Zhou, W., Xie, S.-P. & Yang, D. Enhanced equatorial warming causes deep-tropical contraction and subtropical monsoon shift. *Nat. Clim. Change* **9**, 834–839 (2019).

36. Liu, Z., Vavrus, S., He, F., Wen, N. & Zhong, Y. Rethinking Tropical Ocean Response to Global Warming: The Enhanced Equatorial Warming. *J. Clim.* **18**, 4684–4700 (2005).

37. Lau, W. K. M., Kim, K.-M., Chern, J.-D., Tao, W. K. & Leung, L. R. Structural changes and variability of the ITCZ induced by radiation–cloud–convection–circulation interactions: inferences from the Goddard Multi-scale Modeling Framework (GMMF) experiments. *Clim. Dyn.* **54**, 211–229 (2020).

38. Byrne, M. P. & Schneider, T. Narrowing of the ITCZ in a warming climate: Physical mechanisms. *Geophys. Res. Lett.* **43**, (2016).

39. Donohoe, A., Atwood, A. R. & Byrne, M. P. Controls on the Width of Tropical Precipitation and Its Contraction Under Global Warming. *Geophys. Res. Lett.* **46**, 9958–9967 (2019).

40. Ahmed, F., Neelin, J. D., Hill, S. A., Schiro, K. A. & Su, H. A Process Model for ITCZ Narrowing under Warming Highlights Clear-Sky Water Vapor Feedbacks and Gross Moist Stability Changes in AMIP Models. *J. Clim.* **36**, 4913–4931 (2023).

41. Jeevanjee, N. & Romps, D. M. Mean precipitation change from a deepening troposphere. *Proc. Natl. Acad. Sci.* **115**, 11465–11470 (2018).

42. Murakami, H., Sugi, M. & Kitoh, A. Future changes in tropical cyclone activity in the North Indian Ocean projected by high-resolution MRI-AGCMs. *Clim. Dyn.* **40**, 1949–1968 (2013).

43. Bombardi, R. J. & Boos, W. R. Explaining Globally Inhomogeneous Future Changes in Monsoons Using Simple Moist Energy Diagnostics. *J. Clim.* **34**, 8615–8634 (2021).

44. Bell, S. S., Chand, S. S., Tory, K. J., Ye, H. & Turville, C. North Indian Ocean tropical cyclone activity in CMIP5 experiments: Future projections using a model-independent detection and tracking scheme. *Int. J. Climatol.* **40**, 6492–6505 (2020).

45. Kossin, J. P. Is the North Atlantic hurricane season getting longer? *Geophys. Res. Lett.* **35**, L23705 (2008).

46. Truchelut, R. E. *et al.* Earlier onset of North Atlantic hurricane season with warming oceans. *Nat. Commun.* **13**, 4646 (2022).

47. Goldenberg, S. B., Landsea, C. W., Mestas-Nuñez, A. M. & Gray, W. M. The Recent Increase in Atlantic Hurricane Activity: Causes and Implications. *Science* **293**, 474–479 (2001).

48. Rousseau-Rizzi, R. & Emanuel, K. Natural and anthropogenic contributions to the hurricane drought of the 1970s–1980s. *Nat. Commun.* **13**, 5074 (2022).

49. Dwyer, J. G. *et al.* Projected Twenty-First-Century Changes in the Length of the Tropical Cyclone Season. *J. Clim.* **28**, 6181–6192 (2015).

50. Emanuel, K. Tropical Cyclone Seeds, Transition Probabilities, and Genesis. *J. Clim.* **35**, 3557–3566 (2022).

51. Hsieh, T.-L., Vecchi, G. A., Yang, W., Held, I. M. & Garner, S. T. Large-scale control on the frequency of tropical cyclones and seeds: a consistent relationship across a hierarchy of global atmospheric models. *Clim. Dyn.* **55**, 3177–3196 (2020).

52. Hsieh, T., Yang, W., Vecchi, G. A. & Zhao, M. Model Spread in the Tropical Cyclone Frequency and Seed Propensity Index Across Global Warming and ENSO-Like Perturbations. *Geophys. Res. Lett.* **49**, (2022).

53. Yang, W., Hsieh, T.-L. & Vecchi, G. A. Hurricane annual cycle controlled by both seeds and genesis probability. *Proc. Natl. Acad. Sci.* **118**, e2108397118 (2021).

54. Yamada, Y. *et al.* Evaluation of the contribution of tropical cyclone seeds to changes in tropical cyclone frequency due to global warming in high-resolution multi-model ensemble simulations. *Prog. Earth Planet. Sci.* **8**, 11 (2021).

55. Vincent, E. M. *et al.* Interannual variability of the South Pacific Convergence Zone and implications for tropical cyclone genesis. *Clim. Dyn.* **36**, 1881–1896 (2011).

56. Seager, R. *et al.* Strengthening tropical Pacific zonal sea surface temperature gradient consistent with rising greenhouse gases. *Nat. Clim. Change* **9**, 517–522 (2019).

57. Wing, A. A. & Emanuel, K. A. Physical mechanisms controlling self-aggregation of convection in idealized numerical modeling simulations. *J. Adv. Model. Earth Syst.* **6**, 59–74 (2014).

58. Ferreira, R. N. & Schubert, W. H. Barotropic Aspects of ITCZ Breakdown. *J. Atmospheric Sci.* **54**, 261–285 (1997).

59. Wang, C. & Magnusdottir, G. ITCZ Breakdown in Three-Dimensional Flows. *J. Atmospheric Sci.* **62**, 1497–1512 (2005).

60. Byrne, M. P., Pendergrass, A. G., Rapp, A. D. & Wodzicki, K. R. Response of the Intertropical Convergence Zone to Climate Change: Location, Width, and Strength. *Curr. Clim. Change Rep.* **4**, 355–370 (2018).

61. Delworth, T. L. *et al.* SPEAR: The Next Generation GFDL Modeling System for Seasonal to Multidecadal Prediction and Projection. *J. Adv. Model. Earth Syst.* **12**, (2020).

62. Roberts, M. J. *et al.* Projected Future Changes in Tropical Cyclones Using the CMIP6 HighResMIP Multimodel Ensemble. *Geophys. Res. Lett.* **47**, (2020).

63. Song, F. *et al.* Emergence of seasonal delay of tropical rainfall during 1979–2019. *Nat. Clim. Change* **11**, 605–612 (2021).

64. Wodzicki, K. R. & Rapp, A. D. Long-term characterization of the Pacific ITCZ using TRMM, GPCP, and ERA-Interim. *J. Geophys. Res. Atmospheres* **121**, 3153–3170 (2016).

65. Hersbach, H. *et al.* The ERA5 global reanalysis. *Q. J. R. Meteorol. Soc.* **146**, 1999–2049 (2020).

66. Knapp, K. R., Kruk, M. C., Levinson, D. H., Diamond, H. J. & Neumann, C. J. The International Best Track Archive for Climate Stewardship (IBTrACS): Unifying Tropical Cyclone Data. *Bull. Am. Meteorol. Soc.* **91**, 363–376 (2010).

67. Taylor, K. E., Stouffer, R. J. & Meehl, G. A. An Overview of CMIP5 and the Experiment Design. *Bull. Am. Meteorol. Soc.* **93**, 485–498 (2012).

68. Mizuta, R. *et al.* Climate Simulations Using MRI-AGCM3.2 with 20-km Grid. *J. Meteorol. Soc. Jpn. Ser II* **90A**, 233–258 (2012).

69. Yoshida, K., Sugi, M., Mizuta, R., Murakami, H. & Ishii, M. Future Changes in Tropical Cyclone Activity in High-Resolution Large-Ensemble Simulations. *Geophys. Res. Lett.* **44**, 9910–9917 (2017).

70. Zhang, G., Murakami, H., Knutson, T. R., Mizuta, R. & Yoshida, K. Tropical cyclone motion in a changing climate. *Sci. Adv.* **6**, eaaz7610 (2020).

71. Murakami, H. *et al.* Future Changes in Tropical Cyclone Activity Projected by the New High-Resolution MRI-AGCM. *J. Clim.* **25**, 3237–3260 (2012).

Supplementary Materials for

Warming-induced Contraction of Tropical Convection Delays and Reduces Tropical Cyclone Formation

Gan Zhang

[1]Department of Atmospheric Sciences
University of Illinois at Urbana-Champaign
1301 W. Green Street, Urbana, IL 61801

Corresponding Author
Gan Zhang (gzhang13@illinois.edu)

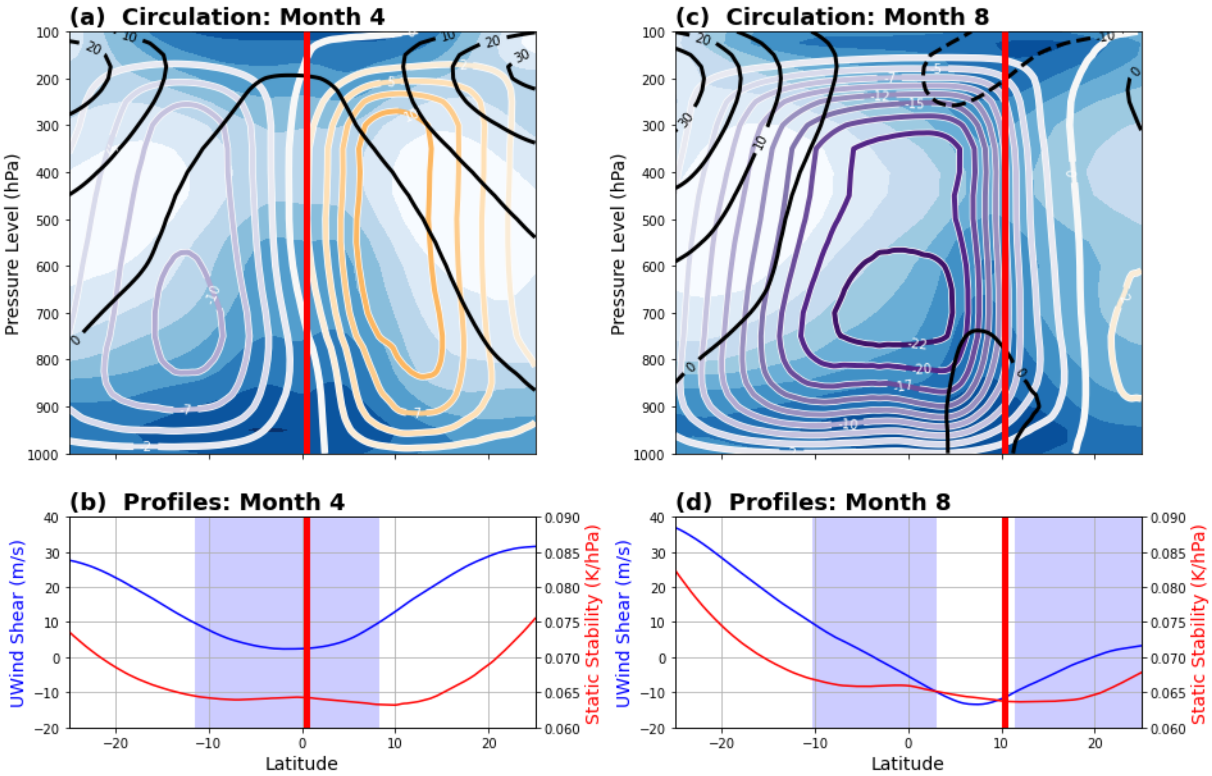

***Supplementary Figure 1** Seasonal variations of the Hadley Circulation and the zonally averaged large-scale environment. (a) April climatology (1981-2010) of the meridional mass streamfunction (10^{10} kg s^{-1}; orange and purple contours), the zonal wind (m s^{-1}), and the relative humidity (%; blue shading). For the streamfunction, the positive values (orange) indicate clockwise motion, and the negative values (purple) indicates counter-clockwise motion. The meridional gradient of the streamfunction is proportional to the strength of vertical motion. The red line marks the latitude of the climatology ITCZ in the corresponding month. (b) April climatology of the vertical shear (blue) of zonal wind (200 hPa – 850 hPa) and the static stability (150 hPa – 850 hPa). The blue shading highlights the latitudes with the magnitude of wind shear smaller than 10 m s^{-1}*. *(c) Same as (a), but for August climatology. (d) Same as (b), but for August climatology.*

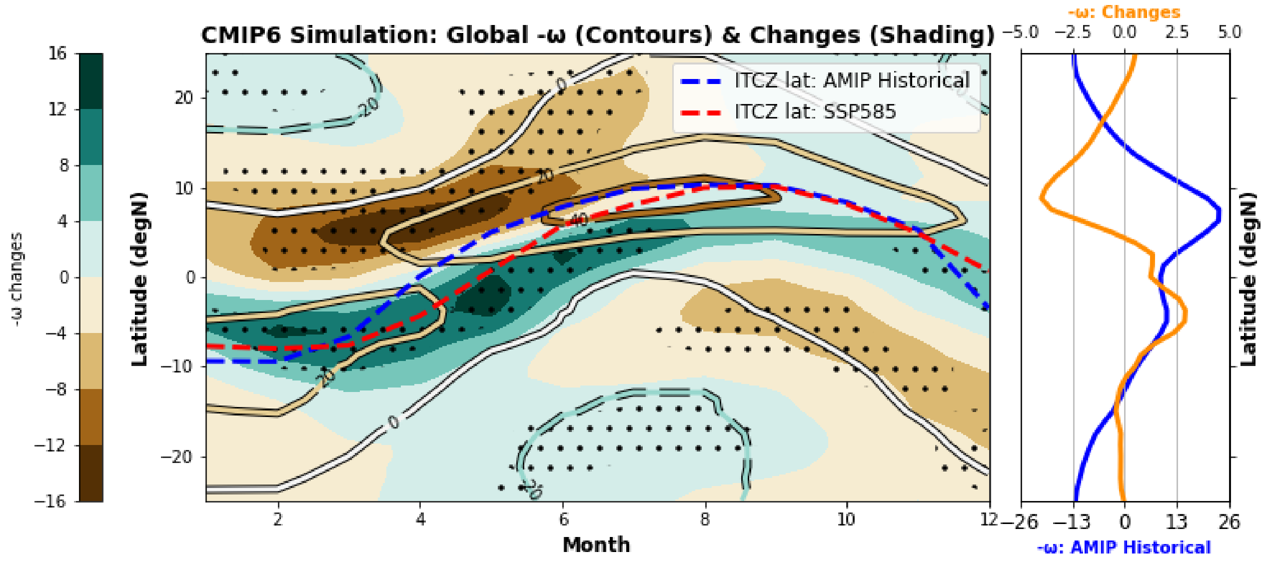

Supplementary Figure 2 *Same as Figure 1b, but for the convection changes simulated by twelve selected CMIP6 models (see Methods).*

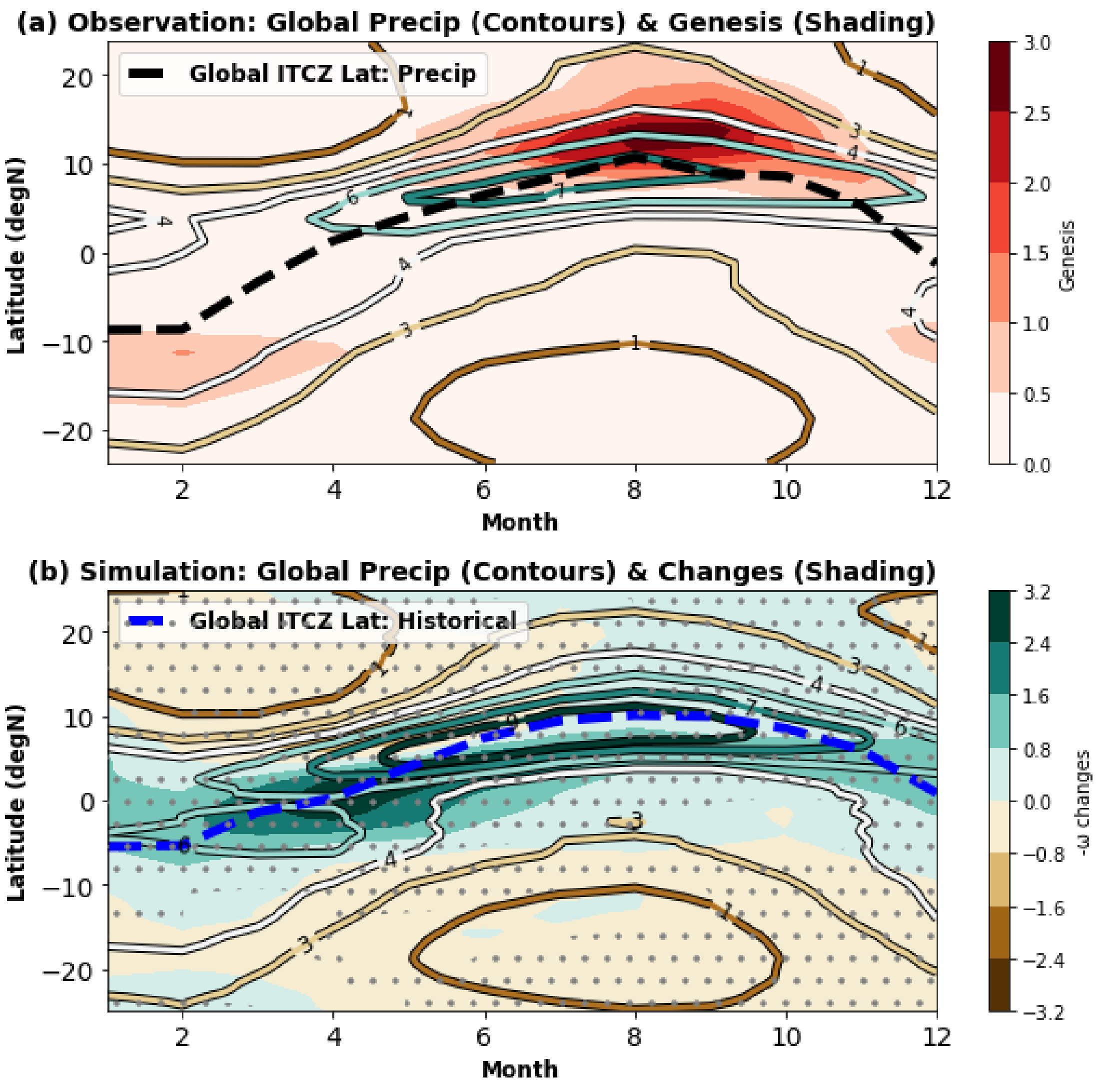

Supplementary Figure 3 *Same as Figure 1a-b, but with the vertical motion replaced with the precipitation (mm day*$^{-1}$*). The precipitation observation is the 2.5-degree gridded data from the Global Precipitation Climatology Project (GPCP) (Adler et al. 2003).*

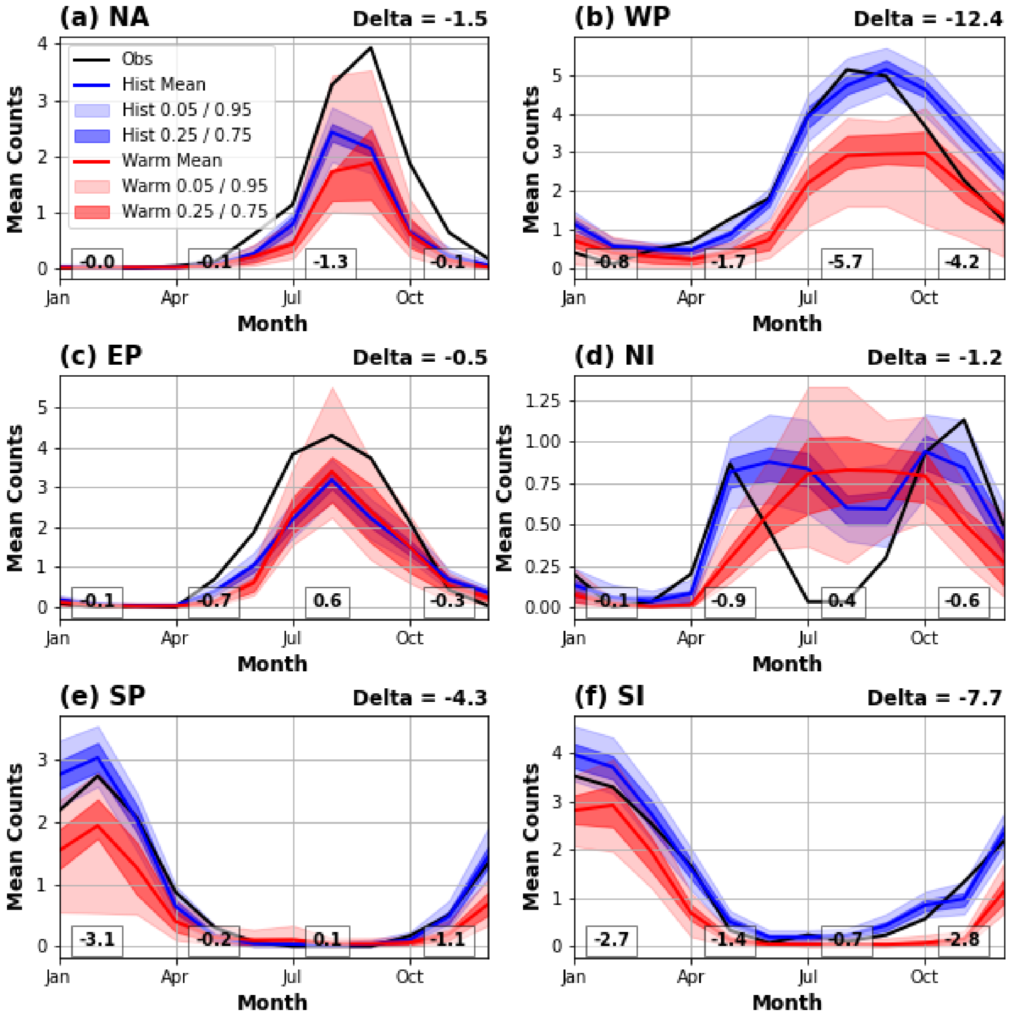

Supplementary Figure 4 *Seasonal cycle of TC activity in six basins. The TC frequency (yr^{-1}) in (a) North Atlantic, (b) Northwestern Pacific, (c) Northeastern Pacific, (d) North Indian Ocean, (e) South Pacific, and (f) South Indian Ocean is separately evaluated for the historical (blue) and the warming (red) experiments. The light and dark shading indicates the 5th-95th percentile range and the 25th-75th percentile range. The black solid line shows the observation values during 1981-2010. The changes in the annual TC frequency are denoted in the upper right of subplots. The changes aggregated over three-month periods (Jan-Mar, Apr-Jun, Jul-Sep, and Oct-Dec) are denoted at the bottom of subplots.*

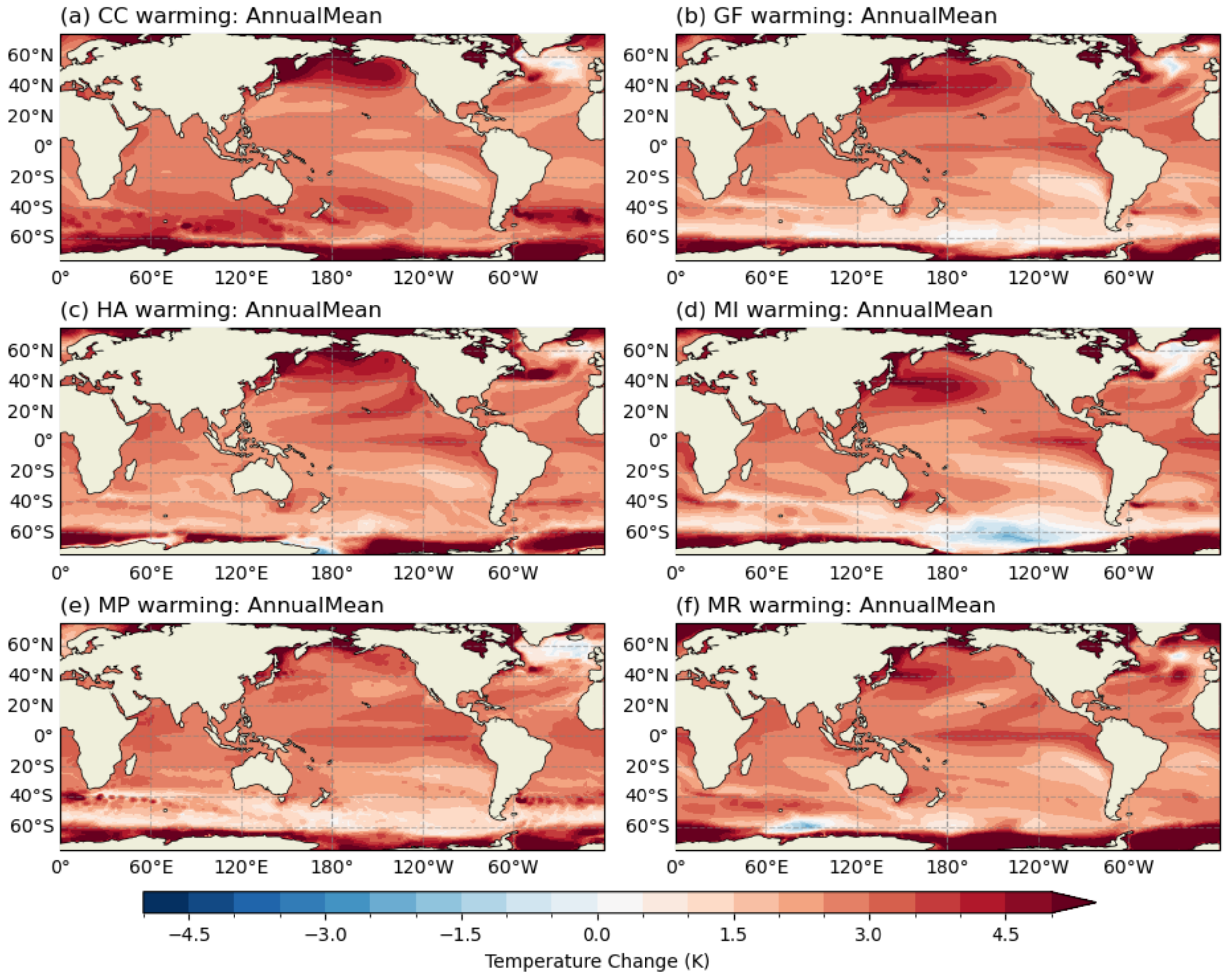

Supplementary Figure 5 *Surface temperature differences between the historical (1981-2010) and 4-K warming (2081-2110) simulations. The annual means of seasonally varying patterns that are scaled from the patterns of (a) NCAR-CCSM4 (CC), (b) GFDL-CM3 (GF), (c) HadGEM2-AO (HA), (d) MIROC5 (MI), (e) MPI-ESM-MR (MP), and (f) MRI-CGCM3 (MR). The strong warming in polar regions is related to sea ice melting.*

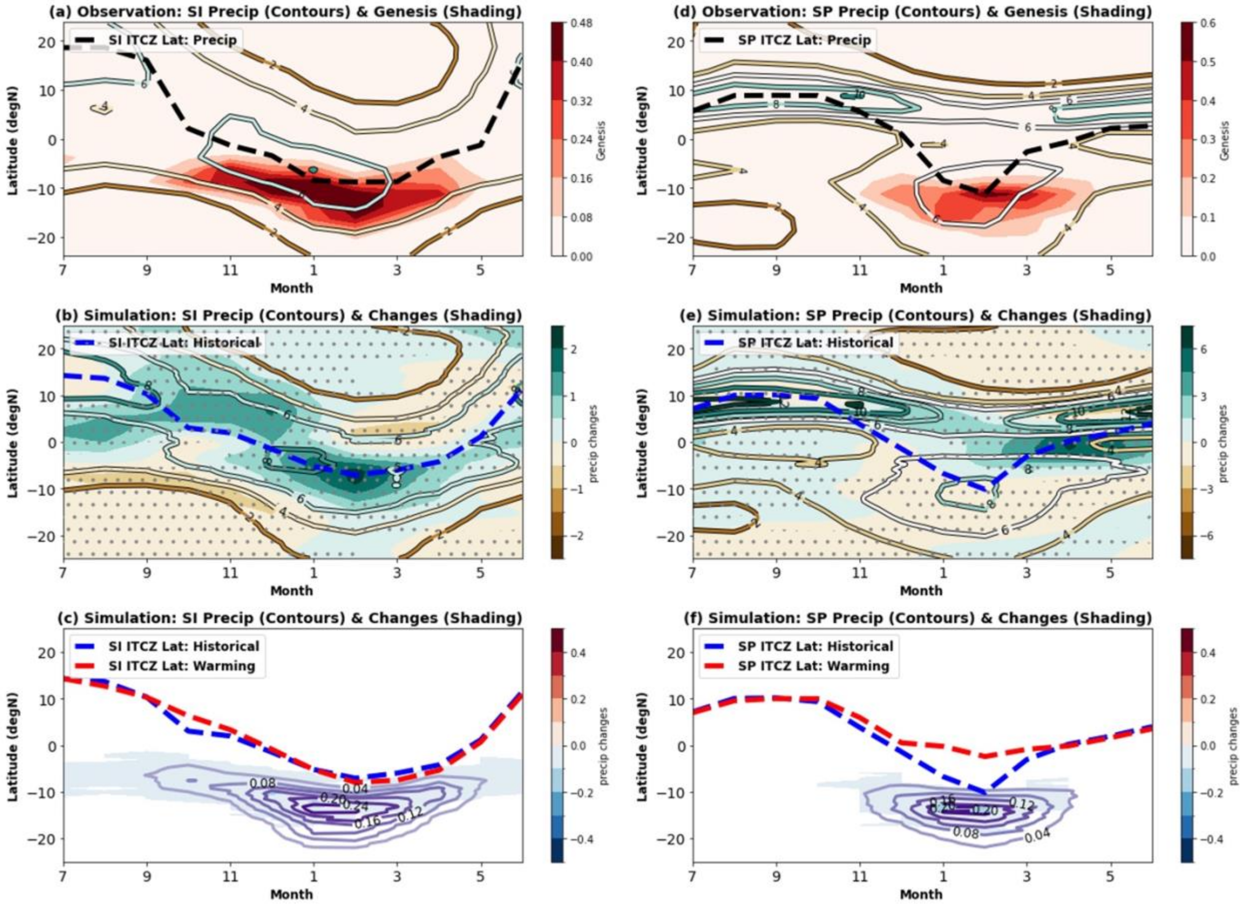

Supplementary Figure 6 *Same as Figure 1 but showing the results in (a-b) the South Indian basin and (c-d) the South Pacific basin. The vertical motion is replaced with precipitation (mm day^{-1}).*

Supplementary Reference

1. Adler, R. F., G. J. Huffman, A. Chang, R. Ferraro, P. Xie, J. Janowiak, B. Rudolf, U. Schneider, S. Curtis, D. Bolvin, A. Gruber, J. Susskind, P. Arkin, and E. Nelkin, 2003: The version 2 Global Precipitation Climatology Project (GPCP) monthly precipitation analysis (1979-present). J. Hydrometeor, 4(6), 1147-1167.